# Supplementary Materials

# Understanding Reaction Networks through Controlled Approach to Equilibrium Experiments using Transient Methods

Yixiao Wang[1], Jin Qian[2,3], Zongtang Fang[1], M. Ross Kunz[1], Gregory Yablonsky[4], Alessandro Fortunelli[2,5], William A. Goddard III[2*], Rebecca R. Fushimi[1*]

[1]Biological and Chemical Science and Engineering Department, Idaho National Laboratory, Idaho Falls, Idaho 83415, United States

[2]Materials and Process Simulation Center, California Institute of Technology, Pasadena, California 91125, United States

[3]Chemical Sciences Division, Lawrence Berkeley National Laboratory, Berkeley, California 94720, United States

[4]Department of Energy, Environmental and Chemical Engineering, Washington University in St. Louis, Saint Louis 63130, United States

[5]CNR-ICCOM, Consiglio Nazionale delle Ricerche, Pisa 56124, Italy

*Correspondence authors: Rebecca.fushimi@inl.gov; wag@caltech.edu

## 1. Catalyst preparation and characterization

Polycrystalline iron (99.99% purity, particle size 450 µm) and cobalt (99.9% purity, particle size 600 µm) were purchased from GoodFellow and Alfa Aesar; respectively. The bimetallic CoFe sample was prepared by wet impregnation of cobalt (II) nitrate hexahydrate, $Co(NO_3)_2 \cdot 6H_2O$ (99.999% purity, Sigma Aldrich) onto the polycrystalline iron sample. The BET area of Fe and Co were determined by $N_2$ adsorption at -196 °C (Tristar II 3020) Micromeritics. The catalyst samples were pre-treated by degassing at 200 °C for 16 h in vacuum (0.05 mbar). The amount of Co loading of CoFe sample was measured by Inductively Couple Plasma Optical Emission Spectroscopy (ICP-OES). The powder X-Ray diffraction (XRD) was recorded by a Bruker-AXS D5005 with a Cu Kα source to obtain the structure of Co and Fe used in this study. The morphology of Fe, Co and CoFe were measured by Transmission Electron Microscopy (TEM) on a JEM-2100P electron microscope operating at 200 kV.

## 2. Methods

### 2.1. Computational

All surface calculations, including geometric optimization and free energy correction were carried out with the Vienna Ab-initio Simulation Package (VASP).[1] We used the Perdew–Burke–Ernzerhof (PBE)[2] formulation of the generalized gradient approximation (GGA) exchange-correlation functional using the projector-augmented (PAW) method and including the D3 (Grimme, Becke, and Johnson)[3] empirical corrections for long-range London dispersion.[4] We used a plane-wave basis set cutoff of 600 eV. We sampled reciprocal space by a Γ-centered Monkhorst–Pack scheme with 3 x 3 x 1 for all calculations. The (111) surface of Co and (110) surface of Fe were chosen based on the most favorable surface energetics:

the (111) surface for an FCC metal, and the (110) surface for a BCC metal. This type of assumptions is frequently adopted to represent the most dominant surfaces and the dominant catalytic behavior. This assumption is also supported experimentally. Figure S8F shows the XRD pattern collected for the Fe, CoFe and Co samples. Fe and Co samples were recorded at 550 °C, which was the same as catalytic test condition. The CoFe sample was recorded at room temperature. The pattern for Fe showed the structure of cubic α-Fe with (110) as the predominant peak, and the pattern of Co showed the predominant cubic structure with the (111) crystal plane in greatest exposure. The PBE-D3(BJ) level of DFT leads to a calculated lattice parameter of a = 2.82 Å for the bulk BCC-Fe structure at 0 K, and a lattice parameter of a = 2.66 Å for the bulk FCC-Co structure.[5] The transition from HCP-Co to FCC-Co is around 700K,[6] so we chose to study Co in the FCC structure because the experimental temperature (450-550 °C) is always above the transition temperature. We chose to study closest packed surfaces, and specifically Fe-BCC(110) and Co-FCC(111), because of their abundance and most favorable surface energies for bare systems,[7] but we also include results from a previous study [12] using identical calculation parameters on N-covered Fe-BCC(111) surface to simulate the nitridation phenomena which occurs on Fe-based catalysts [10]. We include 15 Å of vacuum in the z direction to minimize possible interactions between the replicated cells. The top three layers are relaxed while the bottom three layers were kept fixed.

Calculations for the gas phase molecules used the PBE functional (as implemented in Jaguar) with the D3 empirical correction for London dispersion.[3] To obtain the total free energy, G=H-TS, for the gas molecules at temperature T, we added to the DFT electronic energy (E), the zero-point energy (ZPE) from the vibrational levels (described as simple harmonic oscillators), and the specific heat corrections in the enthalpy from 0 to T. The entropy (S) was evaluated from the same vibrational levels. To correct the free energy for pressure we assumed an ideal gas and added RT*ln(P2/P1) with a reference pressure of P1=1 atm. We used $P_{NH3}$= 25 pascal = $2.5*10^{-4}$ atm, $P_{N2}$= $1.3*10^{-10}$ atm, $P_{H2}$= $1.3*10^{-10}$ atm for this pressure dependent free energy correction.

## 2.2. Experimental

### 2.2.1. TAP reactor

TAP is a high vacuum pulse response technique (base pressure $10^{-8}$ torr) using a pure diffusion reactor to investigate gas-solid interactions and the complex mechanism of catalytic reactions. The thin zone TAP reactor configuration[8] was used to minimize spatial nonuniformities of temperature, gas concentration, and surface concentration. In a TAP experiment, a small amount of gas (ca. 10 nmol/pulse) is injected using a high-speed pulse valve with an electronic trigger duration near 100 μs. These pulsed gas molecules transverse the packed bed via Knudsen diffusion, a random walk, and may adsorb and form products upon interaction with the catalyst surface. Gas/solid interactions are strictly first-order due to the low concentration in the evacuated bed. In the Knudsen diffusion regime, gas phase collisions can be considered negligible. Produce molecules desorbing from the catalyst surface likewise diffuse through the packed bed, eventually escaping when the end of the reactor is encountered where they are recorded as a function of time by a mass spectrometer.

### 2.2.2 Experiments

Fe, CoFe, and Co samples were reduced with 10% $H_2$/Ar flow at 550 °C for about 17 h before being loaded in the TAP reactor. The reactor was predominantly inert quartz particles (210−250 μm) with a thin layer of catalyst at the center. Catalyst samples were exposed to ambient conditions upon loading but were again reduced, now *in situ*, with the same 10% $H_2$/Ar flow at 550 °C overnight. In TAP pulse response experiment, the experiment consists of injecting a small (10 nmol) pulse of the reactant/inert mixture into the evacuated ($10^{-8}$ Torr) packed bed. Gas fills the reactor via Knudsen diffusion and escapes from the exit, where the pulse response is detected with a mass spectrometer. In the Knudsen diffusion regime, only gas-solid collisions are significant. During the gas injection, the chamber pressure was near $10^{-8}$ torr.

Three types of TAP pulse experiments were performed in this study: single gas pulse response, co-pulsed and pump/probe experiments. In the single pulse experiment, a small (10 nmol) pulse of the $NH_3$/Ar mixture (or $H_2$/Ar) was injected into the evacuated ($10^{-8}$ Torr) packed bed with temperature in different experiments ranging from 400 $^oC$ to 550 $^oC$. A course of 20 pulses of the $NH_3$/Ar mixture (40 pulses for $H_2$/Ar) was designed to study the ammonia decomposition (or hydrogen reversible adsorption). For the $NH_3$/Ar pulse experiment, a different atomic mass unit (AMU) was monitored for 3.0 s with progressive cycling between 17, 2, 28 and 40 AMU to record the pulse response for ammonia, hydrogen, nitrogen and argon. In co-pulsed experiments $NH_3$/Ar and $D_2$/Kr mixtures were injected simultaneously from two separate valves ranging from 400 $^oC$ to 550 $^oC$. After each $NH_3$/Ar and $D_2$/Kr co-pulse experiment at a given temperature, the catalyst was regenerated by heating to 550 $^oC$ in order to remove surface adsorbates. In addition, $H_2$/$D_2$ co-pulsed experiments were conducted with $H_2$/Ar and $D_2$ Kr introduced from separate valves. Different AMUs were monitored for 3.0 s cycling between 2, 3, 4, 40, and 84 AMU to record the pulse response for $H_2$, HD, $D_2$, Ar, and Kr. In each co-pulse experiment, a course of 80 gas mixture pulses was performed to study the isotopic exchange.

In pump/probe experiments, two pulse valves were used to consecutively inject pump and probe molecules with varying delay time. For $D_2$/$NH_3$ (or $NH_3$/$D_2$) pump probe Atomic mass unit (AMU) of 2, 3, 4, 17, 18, 19, 28, 40, 84 were recorded for the pulse response of $H_2$, HD, $D_2$, $NH_3$, $NH_2D$, $NHD_2$, Ar, and Kr. The pump probe time spacing was performed at t = 0.2 s, 0.4 s, 0.9 s, and 2.5 s, separately. The pump probe experiments were performed at temperatures of 450, 500, and 550 $^oC$.The pump/probe experiments were performed at temperatures of 450, 500, and 550 $^oC$. In each pump/probe experiment, a measurement of 80 gas pulses was conducted to ensure each gas molecule was represented by 10 data points.

## 2.3. Results

- **Microkinetic Modeling**

From an abstract level, individual chemical reactions happening at the rate *Kij* are denoted as:

$$\sum_{j\in S} \alpha ij\ Sj \overset{Kij}{\longleftrightarrow} \sum_{j\in S} \beta ij\ Sj$$

Where $S\{Sj \in S\}$ is a complete set of chemical species, and $\alpha ij$ , $\beta ij$ are non-negative integers that are directly related to the stoichiometry of the reactants and products. Thus, we can arrange the stoichiometry factors into an $ns$ by $nr$ matrix, where $ns$ stands for the number of chemical species, and $nr$ stands for the number of reactions, and then we can assign rate constant.

We relate the QM formation free energies to the reaction rate constant K, using the Arrhenius equation

$$K = \frac{k_B T * exp\left(\frac{dG}{k_B T}\right)}{h}$$

Thus, for the reaction A+B => C, *the change in the product C's concentration ([C]) would be*

$$\frac{[C]_t}{dt} = [A]_t * [B]_t * K$$

As the reaction proceeds, products from previous reaction serve as the reactants for the subsequent reaction.

*Table S1: Kinetic modeling result of concentration for products and surface species after $NH_3$ decomposition at 550 °C. Initial condition is 1 unit of $NH_3$ in on both Co and Fe after 1 unit of time.*

| | *Fe(110)* | *Co(111)* |
|---|---|---|
| *$NH_3$ (g)* | *2.5E-18* | *1.8E-15* |
| *$NH_3$** | *5.1E-17* | *4.9E-14* |
| *$NH_2$** | *2.4E-11* | *7.9E-11* |
| *NH** | *7.8E-04* | *1.0E-05* |
| *N** | *~1.0E-00* | *2.9E-03* |
| *$N_2$ (g)* | *2.9E-05* | *5.0E-01* |
| *H** | *1.8E-02* | *2.4E-03* |
| *$H_2$ (g)* | *1.5E+00* | *1.5E+00* |

Using the reaction rate constants calculated for different reaction steps reported in Table 1, the output of a mean-field microkinetic model (concentrations of surface and gas species) were numerically calculated after 1 unit of time based on the initial condition of 1 unit of $NH_3$, Table S1. These results shed light on a qualitative estimate of the stable species and their relative concentrations with respect to 1 unit of $NH_3$ as pulse input. The most distinct difference between Fe-BCC(110) and Co-FCC(111) is that Fe stores N* whereas Co produces $N_2$ in larger amount by several orders of magnitude, which is in qualitative

agreement with the experiment across different temperatures. The higher concentration of $NH_2$* and NH*, in combination with the surface D* on Co may serve as the precursor for forming $NH_2D$ and $NHD_2$. Indeed, we observed higher yield of $NH_2D$ and $NHD_2$ on Co(111) at 450 °C. The higher $NH_2D$ and $NHD_2$ production on the Fe catalyst above 550 °C can instead be explained by invoking a higher $NH_3$ decomposition at this higher temperature, leading to a higher coverage in N* adatoms (Fe can store N* as noted above), which in turn gives rise to reshaping of Fe nanoparticle catalysts favoring Fe-BCC(111) and Fe-BCC(100) facets with respect to Fe-BCC(110) facets, as shown in Ref. [9]. Note that on Fe-BCC(111) facets at high N*-coverage the $3N.NH_2$ and $2N.NH_2$ configurations are favored in the resting state, and these configurations can dissociate $D_2$ and then produce $NH_2D$ (mostly, with minor amounts of $NHD_2$).

- **$H_2$ and $NH_3$ Pulsing Arrhenius Plot**

Integral quantities of pulse-response data can be used to characterize the chemicokinetic behavior of a catalyst without assumption of any reaction mechanism. [10] For $H_2$ pulse response experiments, the average value of *reactivities* were calculated from integral quantities of the pulse response (moments) at different temperatures. This data was then used to calculate $k_a$ and $k_d$ according to methods reported by Shekhtman *et al.* [10] as well as Constales *et al.* [11] (Equations S1 and 2 ). An Arrhenius style plot of $k_a$ and $k_d$ are show in Figure S1.

$$k_d = \frac{|r1|}{|r2|} \textit{ (Equation S 1)}$$

$$k_a = k_d * |r1| \textit{ (Equation S 2)}$$

where r1 and r2 is first and second kinetic coefficient.

TAP is rooted in the concept of insignificant perturbation and the simplicity of the measurement brings it closer to that of an elementary step, therefore, first order kinetic can be assumed on the reaction between $NH_3$ and catalyst surface. Under the assumption of first order reaction, the correlation between rate constant and the conversion of reactant is shown in Equation S3 and described in greater detail by Phanawadee *et al.* [12].

$$X = \frac{k_{app} * \tau_{res,cat}^{diff}}{1 + k_{app} \tau_{res,cat}^{diff}} \quad \text{(Equation S3)}$$

Therefore, an Arrhenius style plot can be obtained as show in shown in Figure S1, according to Equation S4,

$$lnk_{app} = ln(A) - \frac{E_a}{R}\left(\frac{1}{T}\right) \quad \text{(Equation S 4)}$$

Based on the slope of the Arrhenius plot, the activation energy on different catalysts can be calculated (Equation S5),

$$Ea = slope * 8.314 \textit{ (Equation S 5)}$$

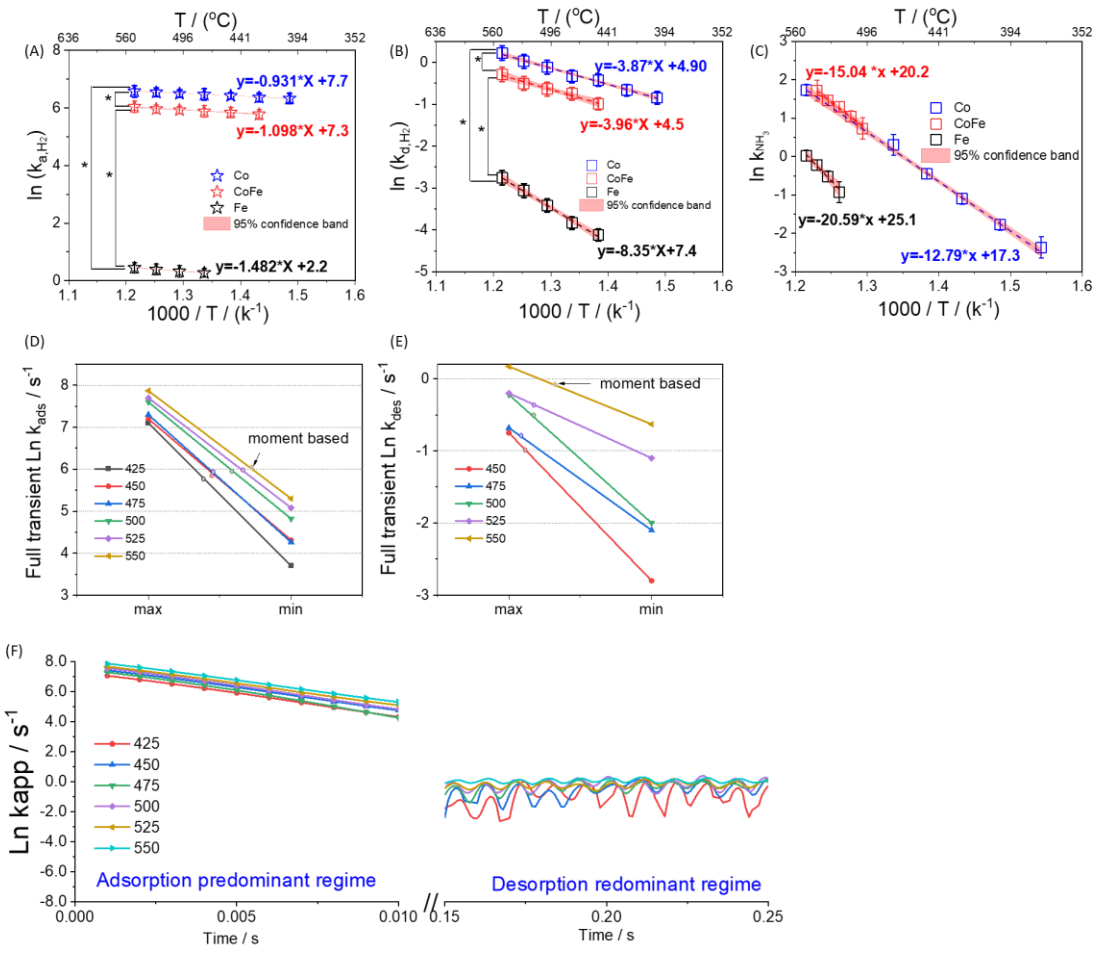


*Figure S1. Arrhenius plot of (A) $H_2$ adsorption, (B) $H_2$ desorption from $H_2$ pulse response experiments and (C) $NH_3$ conversion from $NH_3$ pulse response experiments at different temperatures over different catalysts*. Full transient (D) Ln $k_a$ and (E) Ln $k_d$ as compared to that from moment-based method and (F) Ln $k_{app}$ versus time in a pulse at adsorption and desorption predominant regimes over CoFe at different temperatures. Full transient data and moment-based model is present as (lines + symbols) and circles, respectively. note: $K_a$ was rescaled with the ratio of catalyst surface area and void space of the reactor to obtain the unit of $s^{-1}$.

Besides the moment-based method, the transient data of rate and gas concentration can be used to calculate the transient kinetic constants. Take the CoFe sample as an example, the kinetic constants of $k_a$ and $k_d$ derived from the full transient data are shown in Figures S1D and E. The rate constants derived from these two different models and their correlation indicate that the kinetic constant derived from the moment-based model is in the range of that from the full transient data model.

$k_a$ from the full transient model was calculated with the first 10 data points (Figure S1E) where a negligible amount of surface H coverage was assumed. Therefore, Equation S6 can be simplified as Equation S7, and the $k_{app}$ can be approximated as $k_a$.

$$R = k_a * C * (1 - \theta) - K_d * \theta \quad \text{(S6)}$$

$$R = k_a * C \quad \text{(S7)}$$

$k_{app}$, $k_a$ and $k_d$ is apparent rate constant, adsorption rate constant and desorption rate constant, respectively, with the unit of $s^{-1}$. R is hydrogen rate with the unit of molecules/s/cm$^2$ and C is hydrogen

gas concentration with the unit of molecules/cm$^3$. θ is the surface hydrogen uptake with the unit of molecules/cm$^2$.

$k_d$ from the full transient model was calculated using the data between 0.15 s and 0.25 s where gas concentration is largely eliminated, and desorption rate is higher than the signal-to-noise level. During the time range of 0.15 s to 0.25 s, Equation S6 can be simplified as Equation S8. Therefore, the $k_{app}$ can be approximated as $k_d$.

$$R = -k_d * \theta \qquad (S8)$$

Therefore, the method using the full transient model will bring in larger errors than the moment-based model. These errors can be attributed to the assumptions of low H surface coverage, low $H_2$ gas concentration, and the noise of the single transient data point. Therefore, in this manuscript we use the kinetic constants derived from moment-based method to compare them with DFT results.

The obtained activation energy of $H_2$ adsorption and desorption were plotted together with the activation barrier obtained from DFT calculations (Figure S2A). The obtained $NH_3$ decomposition activation energy from Figure S1 were compared with the activation energy of nitrogen formation step from DFT calculations (Figure S2B).

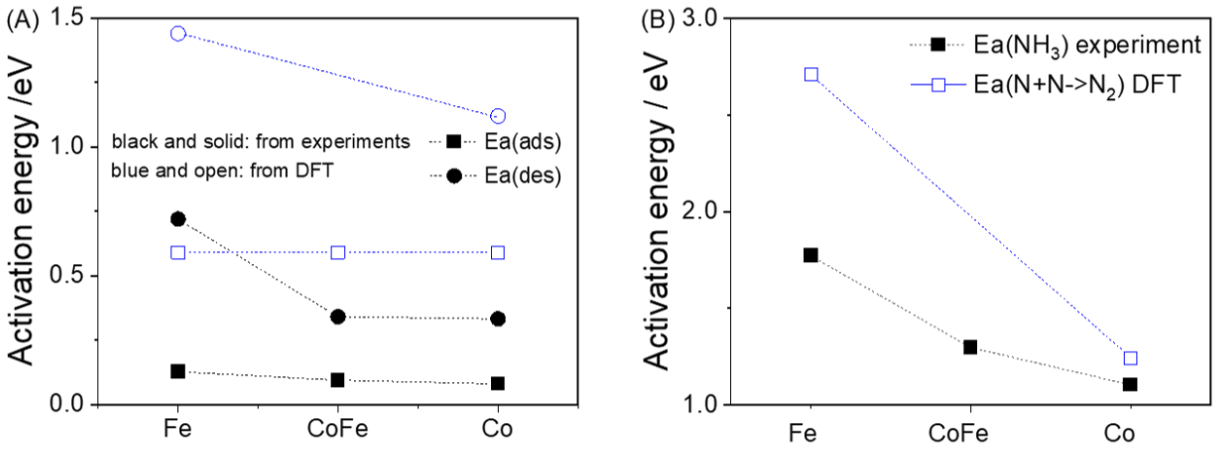


*Figure S2. Activation energy of (A) $H_2$ adsorption and desorption determined from TAP experiements, entropy change and DFT calculations, and (B) ammonia conversion activation energy determined from TAP experiements and $N_2$ formation determined from DFT calculations.*

- **$H_2$/$D_2$ CoPulsing Experiments**

$H_2$/$D_2$ copulsing experiments were conducted to examine the extent of reversible dissociative adsorption. Clear responses of HD were observed on catalysts which demonstrate that hydrogen adsorption was reversible for all materials. Greater HD formation was observed on the CoFe and cobalt materials in comparison to iron (Figure S3).

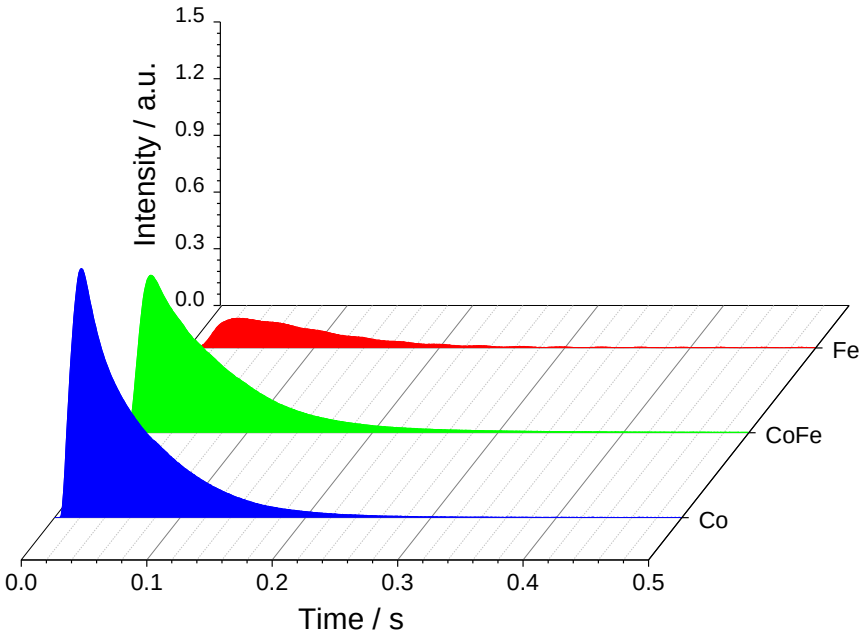


*Figure S3. Mass spectrum pulse response of HD formed during $H_2$ and $D_2$ copusing at 550 °C for each catalyst.*

- **Ammonia Pulse Reversibility**

The rate of ammonia conversion, Figure S4, passes through a singular maximum in response to the inlet pulse. Fe sample demonstrates a small negative reaction rate (black area) which indicates that $NH_3$ is sequentially released from the surface of iron. Simultaneous adsorption/desorption is a possibility for all samples.

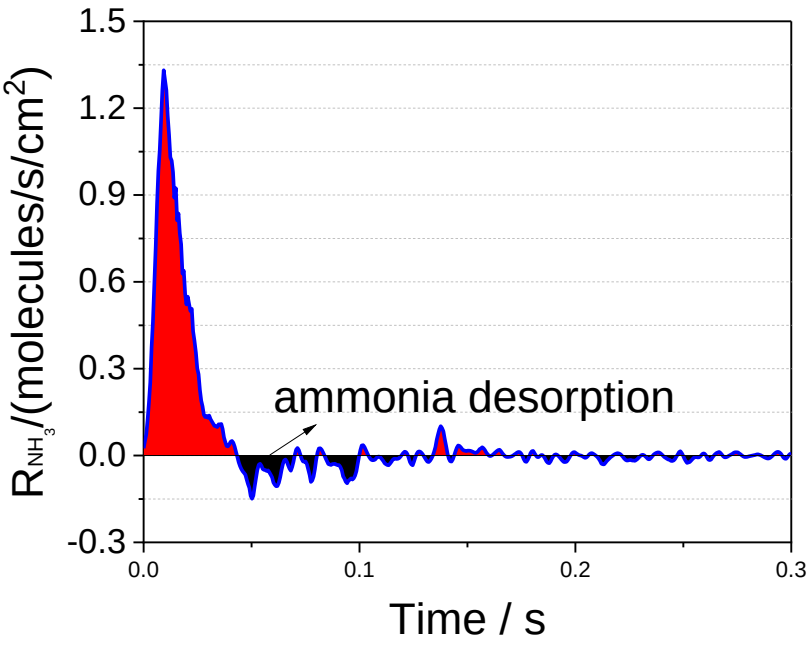


*Figure S4 Transient ammonia reaction rate from pulse response data when ammonia is pulsed over Fe at 550 °C.*

- **Transport Simulation for Co-Pulsed Experiments**

The pulse responses of diffusional transport for $D_2$ and $NH_3$ based on the standard diffusion curve[13] were separately simulated using the same experimental reactor conditions. The simulated reactor outlet flux was then transformed to the catalyst zone concentration time dependence through the use of the G-Procedure described by Kunz et al.[14]. Simulated catalyst zone and reactor outlet concentration time dependences are shown in Figure S5.

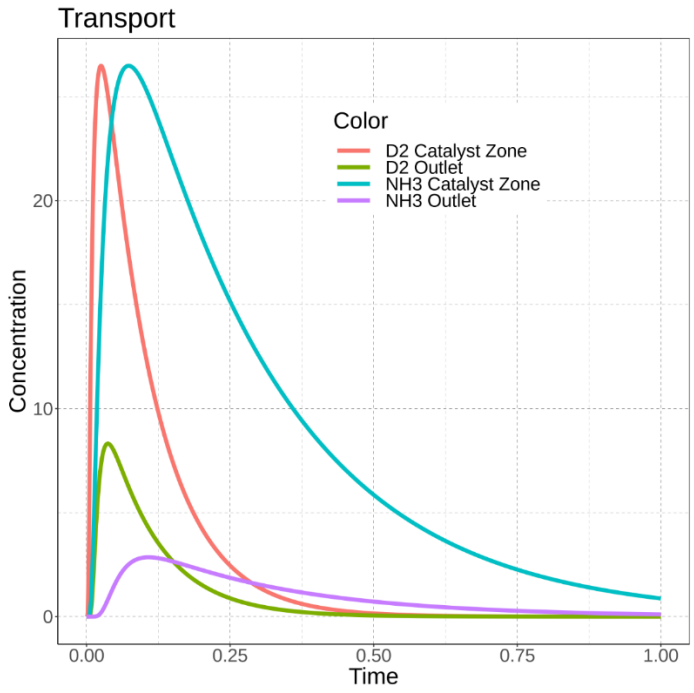


*Figure S5. Simulated $D_2$ and $NH_3$ gas concentration at the catalyst zone*

- **Response of Forward and Reverse Products during Ammonia and $D_2$ copulsing**

*Figure S6* shows the isotopic responses observed for different products released from iron in addition to $H_2$ and minor amounts of $N_2$. This distinct time characteristics of different isotopic products provides evidence of discrete $NH_2^*$, $NH^*$, $H^*$ and $D^*$ species on the iron surface. Similar processes and products in varying amounts were observed over the cobalt material and the CoFe bimetallic. The observation of the mixed isotope products is intriguing as it offers a glimpse of the ammonia *synthesis* steps under unique low-pressure, low-coverage conditions. Although synthesis in this sense is not directly from $N_2$ and $H_2$ we can nonetheless glean information about the hydrogenation process from the rate of formation of $NH_2D$ and $NHD_2$ products.

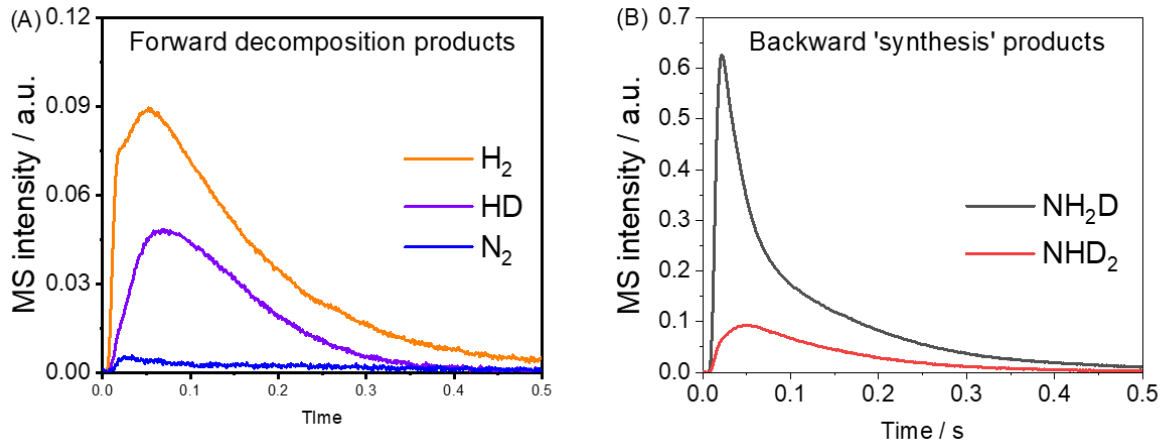


*Figure S6. Product pulse responses detected when $NH_3$ and $D_2$ are co-pulsed over iron at 550 °C. (A) Products resulting from the forward decomposition of ammonia, and (B) products resulting from reversible adsorption of ammonia with isotopic incorporated in bond formation steps.*

- **Half-life Calculations**

From pump/probe experiments the change in product intensity, $C_a$, was recorded as a function of time. An exponential fit of the decay was used to determine a global first order rate constant, $k$, and the associated half-life was determined from:

$$t_{1/2} = \frac{\ln(2)}{k}$$

- **$D_2$ and $NH_3$ pump/probe experiments**

$D_2/NH_3$ pump probe experiments were performed on all samples. For both Co and CoFe, HD was significantly more abundant (intensity around 100 times greater) than $NH_2D$ with simultaneous pulsing. This reflects the favorable nitrogen formation barrier that drives the decomposition forward to reduce the population of $NH_x$ species. With increasing pump/probe delay timing, the depletion of the D* population can be detected in the decay of the HD intensity, leading to a half-life of 1.9 s on CoFe sample (Table 3 in the main text).

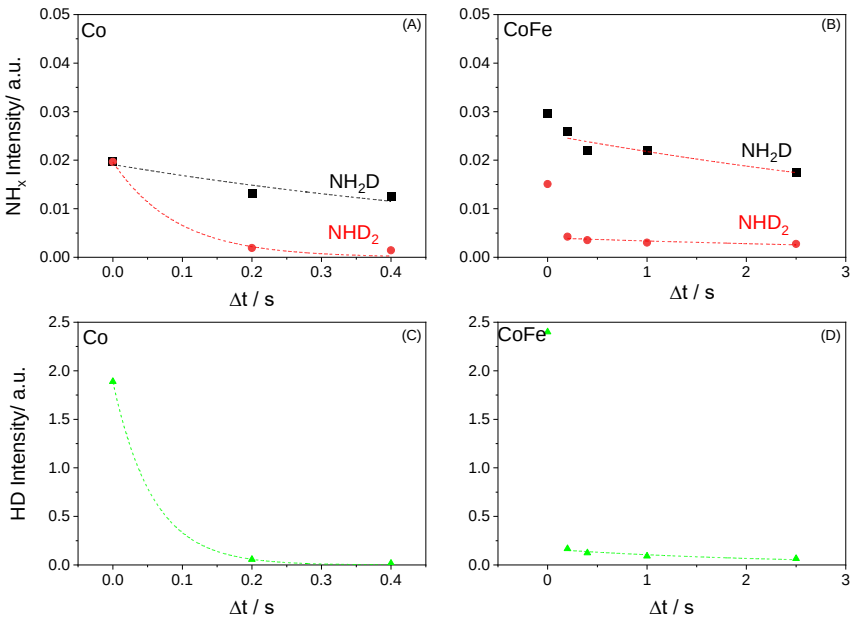


*Figure S7. The normalized intensity (by pulse size) of $NH_2D$, $NHD_2$, and HD intensity versus the pump probe delay time (Δt) cobalt and CoFe.*

- **Catalyst characterization**

Using ICP-OES, the mass loading of Co was 23 wt.%. The BET area of Fe and CoFe were similar and around 4.5 $m^2/g$, whereas it was around 1 for Co. Figure S8A shows the TEM micrographs of CoFe sample, which clearly displayed a cubic morphology of particles of average 94 nm in size (Figure S8B). In order to investigate the morphology and chemical element distributions in the CoFe sample, elemental mapping of CoFe sample was used. The EDX elemental mapping of Co (Figure S8C) showed a uniform distribution of Co over the Fe particle. Fe showed similar particle size and distribution as the CoFe sample. Co appeared to contain large particles in which there are a number of spherical clusters (Figure S8E).

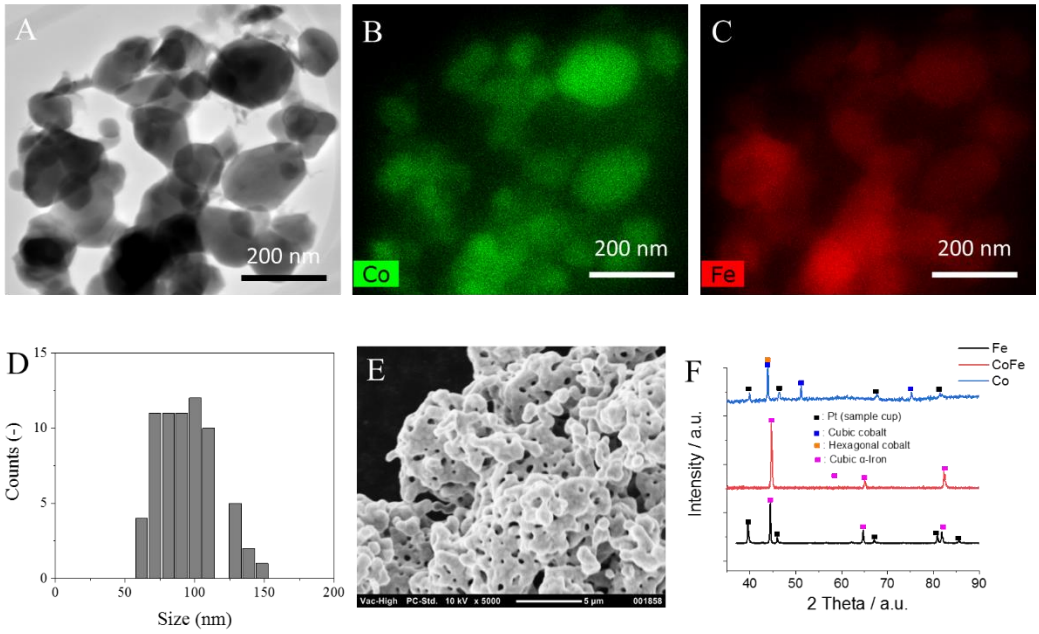


*Figure S8. (A) Representative TEM image of the CoFe sample with (B) Co mapping and (C) Fe mapping. (D) particle size distribution. (E) SEM image of the Co sample. (F) XRD patterns of Fe (at 550 °C), Co (at 550 °C) and CoFe (room temperature).*

## 3. References


1. Kresse, G.; Furthmüller, J., Efficient iterative schemes for ab initio total-energy calculations using a plane-wave basis set. *Physical review B* **1996,** *54* (16), 11169.
2. Hammer, B.; Hansen, L. B.; Nørskov, J. K., Improved adsorption energetics within density-functional theory using revised Perdew-Burke-Ernzerhof functionals. *Physical Review B* **1999,** *59* (11), 7413.
3. Johnson, E. R.; Becke, A. D., A post-Hartree-Fock model of intermolecular interactions: Inclusion of higher-order corrections. *The Journal of chemical physics* **2006,** *124* (17), 174104.
4. Grimme, S.; Antony, J.; Ehrlich, S.; Krieg, H., A consistent and accurate ab initio parametrization of density functional dispersion correction (DFT-D) for the 94 elements H-Pu. *The Journal of chemical physics* **2010,** *132* (15), 154104.
5. Duan, X.; Ji, J.; Qian, G.; Fan, C.; Zhu, Y.; Zhou, X.; Chen, D.; Yuan, W., Ammonia decomposition on Fe (1 1 0), Co (1 1 1) and Ni (1 1 1) surfaces: A density functional theory study. *Journal of Molecular Catalysis A: Chemical* **2012,** *357*, 81-86.
6. Nishizawa, T., T. Nishizawa and K. Ishida, J. Phase Equilibria (formerly Bull. Alloy Phase Diagrams) 4, 387 (1983). *J. Phase Equilibria (formerly Bull. Alloy Phase Diagrams)* **1983,** *4*, 387.
7. Kirklin, S.; Saal, J. E.; Meredig, B.; Thompson, A.; Doak, J. W.; Aykol, M.; Rühl, S.; Wolverton, C., The Open Quantum Materials Database (OQMD): assessing the accuracy of DFT formation energies. *npj Computational Materials* **2015,** *1* (1), 1-15.
8. Shekhtman, S. O.; Yablonsky, G. S.; Chen, S.; Gleaves, J. T., Thin-zone TAP-reactor - theory and application. *Chem. Eng. Sci.* **1999,** *54* (20), 4371-4378.
9. An, Q.; McDonald, M.; Fortunelli, A.; Goddard III, W. A., Controlling the Shapes of Nanoparticles by Dopant-Induced Enhancement of Chemisorption and Catalytic Activity: Application to Fe-Based Ammonia Synthesis. *ACS nano* **2020**.

10. Shekhtman, S. O.; Yablonsky, G. S.; Gleaves, J. T.; Fushimi, R., “State defining” experiment in chemical kinetics—primary characterization of catalyst activity in a TAP experiment. *Chemical engineering science* **2003,** *58* (21), 4843-4859.
11. Constales, D.; Yablonsky, G. S.; Wang, L.; Diao, W.; Galvita, V. V.; Fushimi, R., Precise non-steady-state characterization of solid active materials with no preliminary mechanistic assumptions. *Catalysis Today* **2017**.
12. Phanawadee, P.; Shekhtman, S.; Jarungmanorom, C.; Yablonsky, G.; Gleaves, J., Uniformity in a thin-zone multi-pulse TAP experiment: numerical analysis. *Chemical engineering science* **2003,** *58* (11), 2215-2227.
13. Gleaves, J. T.; Yablonskii, G. S.; Phanawadee, P.; Schuurman, Y., TAP-2: An interrogative kinetics approach. *Applied Catalysis A: General* **1997,** *160* (1), 55-88.
14. Kunz, M. R.; Batchu, R.; Wang, Y.; Fang, Z.; Yablonsky, G.; Constales, D.; Pittman, J.; Fushimi, R., Probability theory for inverse diffusion: Extracting the transport/kinetic time-dependence from transient experiments. *Chemical Engineering Journal* **2020**, 125985.